NUMERICAL SIMULATION OF FLOW ACROSS A COMPLIANT BLUFF BODY IN THE CRITICAL REYNOLDS NUMBER REGIME

Takahide ENDO
Computational Biomechanics Unit,
The Institute of Physical and Chemical Research (RIKEN)
Hirosawa 2-1, Wako-shi, Saitama, 351-0198, Japan
tendo@riken.jp

Ryutaro HIMENO
Computational Biomechanics Unit,
The Institute of Physical and Chemical Research (RIKEN)
Hirosawa 2-1, Wako-shi, Saitama, 351-0198, Japan
himeno@riken.jp

ABSTRACT

A numerical simulation code is constructed for solving flow across a three-dimensional deformable bluff body. It has been reported by several experimental and numerical research works that compliant surface has transition delay of boundary layer and turbulent friction drag reduction effects. However, the mechanism of total drag reduction of flow across a bluff body in the critical Reynolds number regime is not clarified yet. In the present study, numerical analysis of flow across rigid and compliant cylinders in critical Reynolds number regime is performed to evaluate whether compliant surface enhance or suppress boundary layer along the cylinder surface.

INTRODUCTION

A dolphin swims as fast as 40 knots per hour at the maximum. However, its muscles are not sufficiently strong to achieve such fast swimming (Gray, 1936); this is known as "Gray's paradox". Therefore, it is expected that the flexible skin of a dolphin (compliant surface) plays a key role in controlling the surrounding fluid flow. Research studies of compliant surfaces were initiated by Kramer (1960). and it has been reported that deformation of a compliant surface causes transition delay (Gad-el-Hak, 1996; Bushnell *et al.*, 1977; Riley *et al.*, 1988) and friction drag reduction (Kramer, 1960; Chu and Blick, 1969; Endo and Himeno, 2001, 2002).

The application of compliant surface is assumed to be a drag reduction device attached on bluff bodies in flow, such as vehicles, airplanes and ships. Here, flow pattern around a bluff body depends on its Reynolds number. It is well known that the drag coefficient is sharply decreased at critical Reynolds number (drag crisis), where boundary layer along the body becomes turbulent.

The main features of compliant surface which affect on the circumferential fluid field, are the displacement (including the shape of deformation) and deformation velocity. Achenbach and Heinecke (1981) showed small roughness on the cylinder surface makes critical Reynolds number smaller than that for smooth cylinder. Kawamura *et al.*(1986) followed this phenomena via their numerical research. These results indicate that it is possible to obtain drag reduction with small surface roughness by promoting transition of flow, in the shaded region in Figure 1.

On the other hand, many experiments and numerical calculations using the Orr-Sommerfeld equation showed the transition is delayed by deformation of compliant surfaces (Gad-el-Hak, 1996; Bushnell *et al.*., 1977; Riley *et al.*. 1988). Carpenter and Garrad (1985) modeled a compliant surface to an elastic plate which is supported by an array of springs, and found that the transitional Reynolds number increased.

This discrepancy between transition delay with compliant surface and transition enhancement with surface roughness might be originated the deformation velocity of compliant surface. However, the influence of displacement and deformation velocity of compliant surface on surrounding flow is not clarified. And there has been no detailed data of flow around a bluff body with compliant surface in transitional Reynold number regime.

The objective of the present study is to obtain detailed data on the flow field across a deformable compliant bluff body with the aid of numerical simulation. The influence of deformation of compliant surface on the transition phenomena is investigated to clarify whether the transition is enhanced or delayed with compliant coating. The final goal is to examine the correlation between the material properties of the compliant coating on the bluff body and the critical Reynolds number.

NUMERICAL PROCEDURES

The governing equations are the incompressive Navier-Stokes equations and the continuity equation. The deformation of the cylinder is described with a boundary-fitted coordinate system for a moving boundary. The first-order implicit Euler scheme is used to integrate the Navier-Stokes equation.

$$\frac{ ^{n+1} - \ ^{n}}{\triangle t} + \left\{ \left(\ ^{n+1} - \ \ _{t} \right) \cdot \nabla \right\} \ ^{n+1} = -\nabla p + \frac{1}{Re} \triangle \ ^{n+1}, \tag{1}$$

where $\ \ _{t}$ denotes velocity of grid. The second term of the

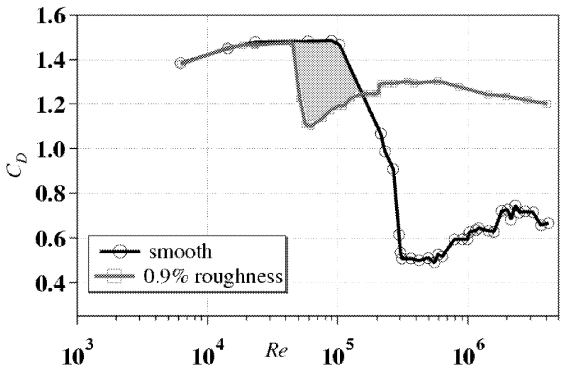

Figure 1: Drag coefficient of the single cylinder with and without roughness. (Achenbach and Heinecke, 1981)

left hand side is linearized for $^{n+1}$ as follows;

$$\frac{^{n+1} - ^{n}}{\triangle t} + \{(^{n} - \quad _t) \cdot \nabla\} \; ^{n+1} = -\nabla p + \frac{1}{Re} \triangle \; ^{n+1}. \tag{2}$$

All spatial derivatives except nonlinear terms in eq. (2) are approximated by 2nd-order central difference method. Nonlinear terms are approximated by the 3rd-order upwind scheme.

The 3rd-order upwind scheme in the curvilinear coordinate system is discretized as follows (Kawamura and Kuwahara, 1985);

$$\begin{aligned}\left(U\frac{\partial u}{\partial \xi}\right)_{i,j,k} &= U_{i,j,k} \quad \frac{-u_{i+2,j,k}+8(u_{i+1,j,k}-u_{i-1,j,k})+u_{i-2,j,k}}{12\triangle\xi} \\ &+ \left|U_{i,j,k}\right| \frac{u_{i+2,j,k}-4u_{i+1,j,k}+6u_{i,j,k}-4u_{i-1,j,k}+u_{i-2,j,k}}{4\triangle\xi},\end{aligned} \tag{3}$$

where U denotes the contravariant velocity.

The nonslip boundary condition is adopted on the cylinder surface. Homogeneous laminar flow is imposed on the upstream side of the outer boundary with the velocity of U_∞, and the 2nd-derivative of the both pressure and velocity field in the streamwise direction is set to be zero on the downstream side of the outer boundary, as schematically shown in Figure 2.

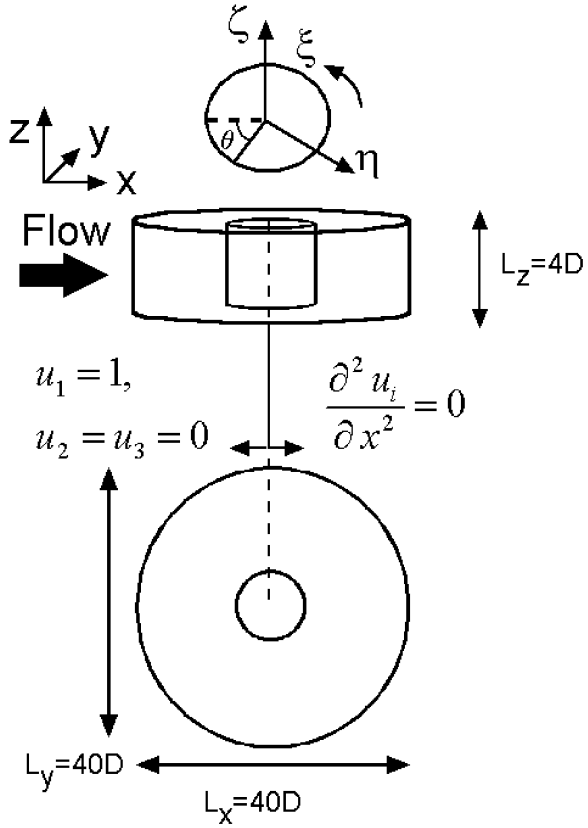

Figure 2: Schematic of calculation domain and coordinate systems.

The measurements for computational volume are $40D$ in the streamwise ($x-$) and in the direction perpendicular to the flow ($y-$), and $4D$ in the spanwise ($z-$) direction which is parallel to the cylinder axis, where D is the diameter of the cylinder. We chose an O-type grid system in the $x-y$ plane, and uniform meshes in the $z-$ direction. A cylindrical coordinate system was also used for ease of comprehension, where $\xi-$ denotes circumferential, $\eta-$ radial, and $\zeta-$ spanwise direction, respectively. The numbers of grid points are $N_\xi = 320, N_\eta = 201$ and $N_\zeta = 80$.

Hereafter, all the parameters are nondimensionalized by U_∞ and D. The computational time step is $\triangle t = 0.001$. The Reynolds number $Re \equiv U_\infty D/\nu$ is $10^3, 10^4, 10^5$ and 10^6. A fully developed instantaneous flow field around a rigid cylinder is used as the initial condition.

MODELING OF COMPLIANT SURFACE

The material property of the compliant surface is assumed to be isotropic. The compliant surface covers a rigid core of the cylinder, as it is schematically shown in Figure 3. Each grid point on the compliant surface is assumed to move only in the radial direction. The compliant coating is modeled by a spring, mass, and damper system. The tensions employed on the compliant coating are neglected for the simplicity. And

the wall displacement d is determined as follows:

$$m\frac{\partial^2 d}{\partial t^2} + c\frac{\partial d}{\partial t} + k(d - d_0) = \triangle\xi\triangle\zeta\left(P_\eta - \tilde{P_\eta}\right), \qquad (4)$$

where m is the mass of a compliant surface for one calculation grid volume, and is determined as $m \equiv \rho_c \cdot \Delta\zeta \cdot \pi\{D^2 - (D - d)^2\}/N_\xi$ (ρ_c is the density of a compliant surface). The parameters c and k are the damping parameter and the spring stiffness. The driving force of the compliant coating is the pressure and friction drag in the radial component, and is defined as;

$$P_\eta \equiv \frac{-\left\{\alpha^{12}\tau_{12} + \alpha^{22}\tau_{22} + \alpha^{23}\tau_{23}\right\}}{\sqrt{(\alpha^{12})^2 + (\alpha^{22})^2 + (\alpha^{23})^2}}, \qquad (5)$$

where $\tau_{ij} = -p\delta_{ij} + (1/Re)\,(u_{i,j} + u_{j,i})$ is a stress tensor; $\alpha^{ij} \equiv (1/J)(\partial\eta^i)/(\partial x_m)\cdot(\partial\eta^j)/(\partial x_m)$ is a metric tensor, and J is the Jacobian of the grid.

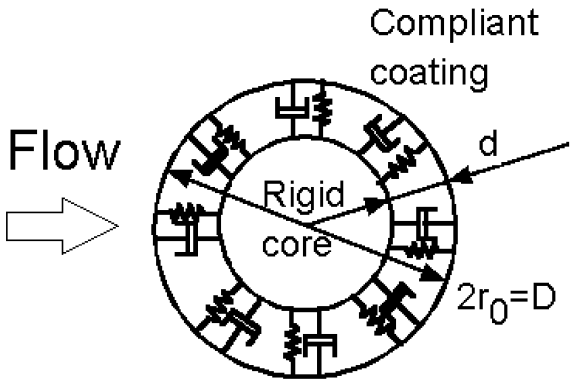

Figure 3: Schematic model for a compliant surface.

We recently calculated flow around a compliant cylinder to investigate the influence of compliant surface on friction drag at low-Reynolds number flow($Re \sim 80$) (Endo and Himeno, 2003). It is found that the pressure drag is increased while the friction drag is decreased, as the projection area of compliant cylinder becomes larger. In the present study, in order to investigate influence of the fluctuation of deformation of compliant surface changing every moment, an ensemble averaged value of driving force ($\tilde{P_\eta}$) on the compliant surface is subtracted from the RHS of eq. (4). And $\tilde{P_\eta}$ is averaged from data of the driving force on the rigid cylinder.

Equation (4) is non-dimensionalized by inlet velocity U_∞ and the cylinder diameter D, as follows;

$$\frac{\partial^2 d}{\partial t^2} + 2\zeta_0\frac{\partial d}{\partial t} + \omega_0^2\left(d - \frac{1}{2}\right) = \frac{1}{\rho}\frac{1}{d(1-d)}\left(P_\eta - \tilde{P_\eta}\right). \qquad (6)$$

The nondimensional density is determined as $\rho \equiv \rho_c/\rho_f$, where ρ_f is fluid density.

It is easily understood that there are several parameters concerned with material properties of compliant surface. And it is difficult to find the optimal combination of these parameters for fluid control.

The final goal of our study is to make a guidance of the optimal combination of these parameters for drag reduction,

(a)

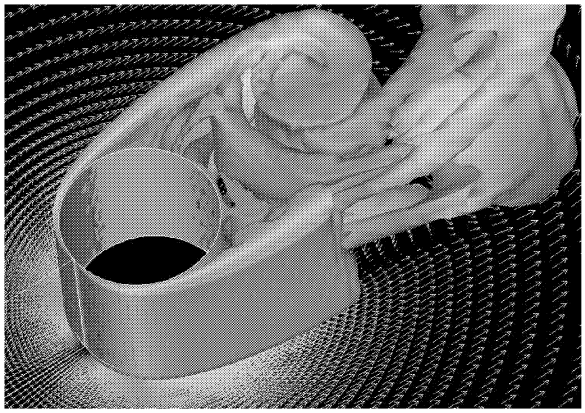

(b)

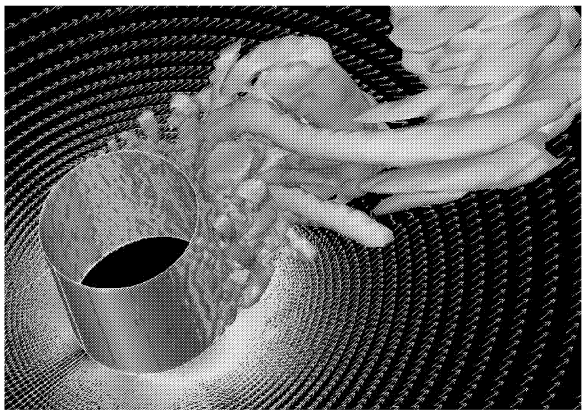

Figure 4: Instantaneous flow field across a rigid cylinder. Contour shows vortical structure. (a) $Re = 10^3$, (b) $Re = 10^6$. 1/4 of the calculation domain in $z-$direction is visualized.

however, since the computational load is quite large to solve flow around a cylinder in the critical Reynolds number regime, parametric study is rather difficult. Therefore, several combination of these parameters are tested in two-dimensional and low Reynolds number flow calculation. Based on the result of two-dimensional calculations, only one combination of parameters is used in the present three-dimensional simulation, and is $\zeta_0 = 40, \omega_0 = 20, \rho = 1, d = 0.2$.

RESULTS AND DISCUSSION

Instantaneous flow fields around rigid cylinder at Reynolds number of 10^3 and 10^6 are shown in Figure 4. Flow is from left-down to right-up. Only 1/4 of the calculation domain in $z-$direction is visualized. Contour shows vortical structure (II=-0.05; II is the second invariant of the deformation tensor) (Chong *et al.*; 1990). Quite complicated vortical structures are observed in the cylinder wake region. As it is well known, three-dimensional structure is dominant, and separation point moves downwards, with Reynolds number becomes larger. Typically at Reynolds number $Re = 10^6$, the wake region becomes quite narrow, which indicates that the wake becomes turbulent.

Figure 5 shows instantaneous flow field across compliant

(a)

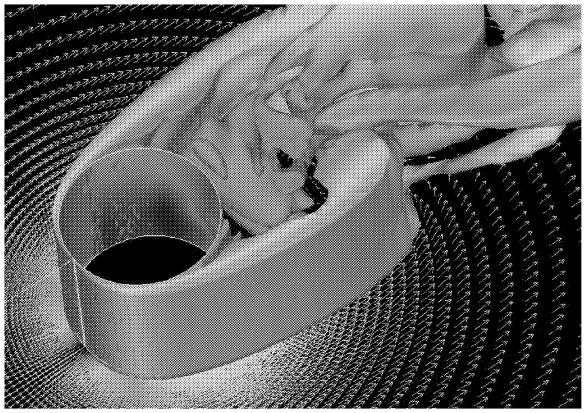

(b)

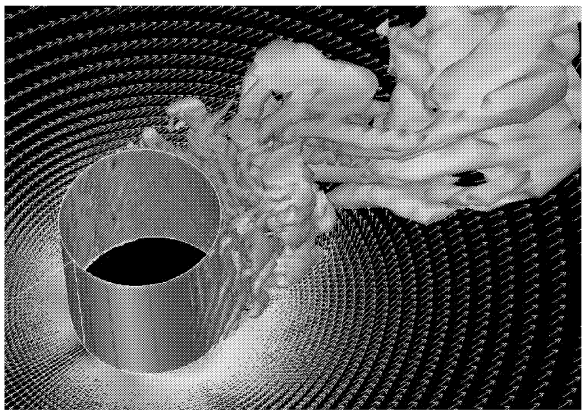

Figure 5: Instantaneous flow field across a rigid cylinder. (a) $Re = 10^3$, (b) $Re = 10^6$.

cylinder. Since the damping parameter (ζ_0) and the spring stiffness (ω_0) used in the present study is large, wall displacement and deformation velocity are very small. Therefore, there observed little difference in the flow fields around rigid and compliant cylinders. It is necessary to investigate the flow with softer compliant surface.

The total drag coefficient of cylinder $C_D \equiv P_\eta / \frac{1}{2}\rho_f U_\infty^2$ can be divided into two parts; the coefficient of pressure drag C_{Dp} and that of friction drag $C_{D\tau}$.

$$C_D = C_{Dp} + C_{D\tau}, \tag{7}$$

Each $x-, y-, z-$ component of pressure and friction drag coefficient is calculated as follows;

$$\begin{bmatrix} C_{Dx} \\ C_{Dy} \\ C_{Dz} \end{bmatrix} = \begin{bmatrix} -p & 0 & 0 \\ 0 & -p & 0 \\ 0 & 0 & -p \end{bmatrix} \begin{bmatrix} \mathbf{e_x^n} \\ \mathbf{e_y^n} \\ \mathbf{e_z^n} \end{bmatrix} + \begin{bmatrix} \frac{2}{Re}\frac{\partial u}{\partial x} & \frac{1}{Re}\left(\frac{\partial u}{\partial y} + \frac{\partial v}{\partial x}\right) & \frac{1}{Re}\left(\frac{\partial u}{\partial z} + \frac{\partial w}{\partial x}\right) \\ \frac{1}{Re}\left(\frac{\partial u}{\partial y} + \frac{\partial v}{\partial x}\right) & \frac{2}{Re}\frac{\partial v}{\partial y} & \frac{1}{Re}\left(\frac{\partial v}{\partial z} + \frac{\partial w}{\partial y}\right) \\ \frac{1}{Re}\left(\frac{\partial u}{\partial z} + \frac{\partial w}{\partial x}\right) & \frac{1}{Re}\left(\frac{\partial v}{\partial z} + \frac{\partial w}{\partial y}\right) & \frac{2}{Re}\frac{\partial w}{\partial z} \end{bmatrix} \cdot \begin{bmatrix} \mathbf{e_x^n} \\ \mathbf{e_y^n} \\ \mathbf{e_z^n} \end{bmatrix}, \tag{8}$$

where, $(\mathbf{e_x^n}, \mathbf{e_y^n}, \mathbf{e_z^n})$ is normal vector on the surface of cylinder.

(a)

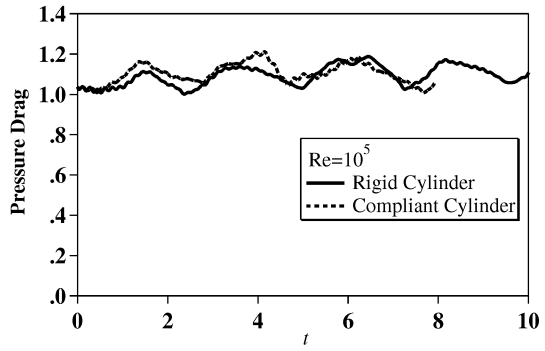

(b)

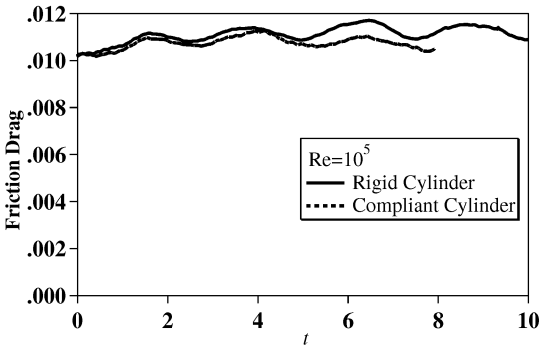

Figure 6: Time traces of (a) pressure drag coefficient C_{px}, and (b) friction drag coefficient $C_{\tau x}$ in $Re = 10^5$.

We call the first term of RHS in eq. (8) as (C_{px}, C_{py}, C_{pz}), the second term $(C_{\tau x}, C_{\tau y}, C_{\tau z})$, hereafter.

Figure 6 shows time traces of pressure drag coefficient C_{px}, and friction drag coefficient $C_{\tau x}$ in $Re = 10^5$ flow. Although the calculated time steps are not sufficiently long, friction drag coefficient is slightly decreased, while pressure drag remains unchanged. Although the friction drag reduction is small, this fact shows that the total drag can be reduced with compliant surface. Furthermore, the present result indicates that significant drag reduction with compliant surface is possible when the friction drag is dominant in the flow around some bodies, such as airplane, ships, and linear motor car.

CONCLUSIONS

We developed a numerical simulation code for various Reynolds number flow across a deformable cylinder. It is found that the pressure drag is almost unchanged, while the friction drag is decreased. The drag coefficients of various Reynolds number flow will be arranged, and the influence of the deformation of compliant surface on transition phenomena of flow across a bluff body is investigated. When the drag crisis occurs lower Reynolds number, drag reduction with compliant surface becomes realistic. It is necessary to investigate the optimal combination of material properties of the compliant surface to decrease both pressure and friction drag. It is also desired to calculate a flow around a streamlined compliant body to examine the applicability of compliant surface as a

practical drag reduction device.

REFERENCES

Achenbach, E., and Heinecke, E., 1981, "On vortex shedding from smooth and rough cylinders in the range of Reynolds numbers 6×10^3 to 5×10^6", *J. Fluid Mech.*, Vol. 109, pp. 239-251.

Bushnell, D. M., Hefner, J. N., and Ash, R. L., 1977, "Effect of Compliant Wall Motion on Turbulent Boundary Layers", *Phys. Fluids*, Vol. 20, pp. S31-S48.

Carpenter, P. W., and Garrad, A. D., 1985, "The hydrodynamic stability of flow over Kramer-type compliant surfaces. Part 1. Tollmien-Schlichting instability", *J. Fluid Mech.,* Vol. 155, pp. 465-510.

Chong, M. S., Perry, A. E., and Cantwell, B. J., 1990, "A general classification of three-dimensional flow fields", *Phys. Fluids*, Vol. A2-5, pp. 765-777.

Chu, H. H., and Blick, E. F., 1969, "Compliant Surface Drag as a Function of Speed", *J. Spacecraft and Rockets,* Vol. 6, pp. 763-764.

Endo, T., and Himeno, R., 2001, "Direct Numerical Simulation of Turbulent Flow Over a Compliant Surface", *Proc. 2nd Int. Symp. Turbulence & Shear Flow Phenomena*, Stockholm, Vol. 1, pp. 395-400.

Endo, T., and Himeno R., 2002, "Direct Numerical Simulation of Turbulent Flow Over a Compliant Surface", *Journal of Turbulence*, Vol. 3, 007.
(http://www.stacks.iop.org/1468-5248/3/007).

Endo, T., and Himeno, R., 2003, "Direct numerical simulation of flow across a compliant bluff body", *Proc. 3rd Int. Symp. Turbulence & Shear Flow Phenomena*, Sendai, Vol. 3, pp. 965-970.

Gad-el-Hak, M., 1996, "Modern Developments in Flow Control", *Appl. Mech. Rev.*, Vol. 49-7, pp. 365-379.

Gray, J., 1936, "Studies in Animal Locomotion. VI The Propulsive Powers of the Dolphin", *J. Exp. Biology*, Vol. 50, pp. 233-255.

Kawamura, T., and Kuwahara, K., 1984, "Computation of high Reynolds number flow around a circular cylinder with surface roughness", *AIAA paper*, 84-0376.

Kawamura, T., Takami, H., and Kuwahara, K., 1986, "Computation of high Reynolds number flow around a circular cylinder with surface roughness", Fluid Dynamic Research, Vol. 1, pp. 145-162.

Kramer, M. O., 1960, "Boundary Layer Stabilization by Distributed Damping", *Nav. Eng. J.*, Vol. 72, pp. 25-33.

Riley, J. J., Gad-el-Hak, M., and Metcalfe, R. W., 1988, "Compliant Coatings", *Annu. Rev. Fluid Mech.,* Vol. 20, pp. 393-420.